Adv Syst Sci Appl 2021; **03**:75–90
Published online at https://ijassa.ipu.ru.

Applications of Sine-Cosine Wavelets Method For Solving Drinfel'd–Sokolov–Wilson System

Naser Azizi[1], Reza Pourgholi[1*]

[1] *School of Mathematics and Computer Science, Damghan University, Damghan, Iran*

Abstract: In this article, we use the Sine-Cosine wavelets (SCWs) method to numerically solve the Drinfel'd–Sokolov–Wilson (DSW) system. For this purpose, we use an approximation of functions with the help of SCWs, and we approximate spatial derivatives using this method. The operational matrix based on SCWs has a large number of zero components, which ensures good system performance and provides acceptable accuracy even with fewer collocation points. In the end, to show the effectiveness and accuracy of the method in solving this system one numerical example is provided.

Keywords: Drinfel'd–Sokolov–Wilson system, numerical method, sine-cosine wavelets method, operational matrix

1. INTRODUCTION

Nonlinear coupled partial differential equations (PDEs) are very significant in a type of scientific field, especially in fluid mechanics, solid-state physics, plasma waves, plasma physics, and chemical physics. Since many nonlinear physical phenomena can be explained by the exact and numerical solutions of nonlinear equations, the attempt for finding the exact and numerical solutions to these phenomena is important.

In this article, our main goal is to solve numerically the DSW system. A generalized form of the DSW system is given by:

$$\begin{cases} \Psi_t + \alpha\Phi\Phi_x = 0, \\ \Phi_t + \beta\Phi_{xxx} + \gamma\Psi\Phi_x + \delta\Psi_x\Phi = 0, \end{cases} \tag{1.1}$$

where α, β, γ, and δ are some nonzero parameters.

System (1.1) plays an important role in fluid dynamics [8,12] and is originally introduced by Drinfel'd and Sokolov [7] and Wilson [24] as a model of dispersive water waves. Many researchers have devoted considerable efforts by successfully implementing various methods to extract solitary wave solutions and other solutions of DSW system [1, 10, 17, 23, 25].

One way to solve equations numerically is to use wavelets. The basic idea of wavelets goes back to the early 1960s [4,5]. There are developments concerning the multiresolution analysis algorithm based on wavelets [6] and the construction of compactly supported orthonormal wavelet bases [16]. So far, several problems have been solved numerically using different wavelets, for example, we can refer to references [2, 3, 9, 13, 18, 19, 26, 27]. In this paper, we consider system (1.1) by using the SCWs method to find numerical solutions. SCW has been used and showed efficiency to solve various problems. To indicate this, we can refer to some

*Corresponding author: pourgholi@du.ac.ir

works. Razzaghi and Yousefi in [20] have employed a SCW to solve variational problems. Tavassoli Kajani et al. [15] for solving integro-differential equations have presented a method based on SCWs. A numerical evaluation of Hankel transform for seismology has been given in [14] using the SCWs approach. Amir and Umer Saeed in [22] have used SCWs to solve the fractional nonlinear oscillator equations.

In the present article, we intend to use the SCWs method to numerically solve the DSW system (1.1) with the initial conditions

$$\Psi(x,0)=f_1(x), \qquad \Phi(x,0)=f_2(x), \qquad x\in[0,1], \tag{1.2}$$

and the boundary conditions

$$\begin{array}{lll} \Psi(0,t)=g_1(t), & \Phi(0,t)=g_2(t), & t\in[0,t_{fin}],\\ \Phi(1,t)=k_2(t), & \Phi_x(0,t)=w_2(t), & t\in[0,t_{fin}], \end{array} \tag{1.3}$$

where t_{fin} represents the final time. The differentiable functions $f_i(x)$, $g_i(t)$, for $i=1,2$, $k_2(t)$, and $w_2(t)$ are known.

The structure of this article is as follows: In Section 2, we describe the properties of the SCWs. In the following, expanding functions into the SCWs series and operational matrix of them for the numerical solutions are discussed. In Section 3, the procedure of implementation of the SCWs method, for system (1.1) with specified initial and boundary conditions (1.2) and (1.3) is presented. The numerical performance of the method is made in Section 4, and finally, concluding remarks are given in Section 5.

2. PROPERTIES OF SCWS

Wavelets are useful mathematical functions constructed from the dilation and translation of a single function called the mother wavelet, which can be denoted by ω. Assuming that the expansion parameter η and the translation parameter ν are considered, we have the continuous wavelets family as follows [11]:

$$W_{\eta,\nu}(x)=|\eta|^{-\frac{1}{2}}\omega\Big(\frac{x-\nu}{\eta}\Big), \qquad \eta,\nu\in\mathbb{R}, \quad \mu\neq 0.$$

If the parameters η and ν are restricted to take values $\eta=\eta_0^{-\kappa}$ and $\nu=r\nu_0 a_0^{-\kappa}$, a family of discrete wavelets is obtained as:

$$W_{\kappa,r}(x)=|\eta_0|^{\frac{\kappa}{2}}\omega(\eta_0^{\kappa}x-r\nu_0), \tag{2.4}$$

where $\eta_0>1$, $\nu_0>0$, and r and κ are positive integers. The set $\{W_{\kappa,r}(x)\}$ in (2.4), forms a wavelet basis for $\mathcal{L}^2(\mathbb{R})$. Especially, if $\eta_0=2$ and $\nu_0=1$, the set $\{W_{\kappa,r}(x)\}$ forms an orthonormal basis.

SCWs are defined on interval $x\in[0,1)$ as [14]:

$$W_{r,s}(x)=2^{\frac{\kappa+1}{2}}\mathscr{G}_s(2^{\kappa}x-r)\chi_{[\frac{r}{2^{\kappa}},\frac{r+1}{2^{\kappa}})}, \tag{2.5}$$

where $\kappa=\{0\}\cup\mathbb{N}$, $r=0,1,2,\ldots,2^{\kappa}-1$, and $\chi_{[\frac{r}{2^{\kappa}},\frac{r+1}{2^{\kappa}})}$ denotes the characteristic function given as

$$\chi_{[\frac{r}{2^{\kappa}},\frac{r+1}{2^{\kappa}})}=\begin{cases}1, & x\in[\frac{r}{2^{\kappa}},\frac{r+1}{2^{\kappa}}),\\ 0, & \text{elsewhere.}\end{cases} \tag{2.6}$$

Also,

$$\mathscr{G}_s(x)=\begin{cases}\frac{1}{\sqrt{2}}, & s=0,\\ \cos(2s\pi x), & s=1,2,\ldots,\ell,\\ \sin(2(s-\ell)\pi x), & s=\ell+1,\ell+2,\ldots,2\ell,\end{cases} \tag{2.7}$$

where ℓ is any positive integer.

SCWs have compact support and are an orthonormal basis for $\mathcal{L}^2([0,1))$. The orthonormal basis functions for SCWs by assuming $\kappa = 1$ and $\ell = 1$ are obtained as follows:

$$\begin{cases} \text{for} \quad 0 \le x < \frac{1}{2} \quad \Longrightarrow \quad \begin{cases} W_{0,0}(x) = \sqrt{2}, \\ W_{0,1}(x) = 2\cos(4\pi x), \\ W_{0,2}(x) = 2\sin(4\pi x), \end{cases} \\ \text{for} \quad \frac{1}{2} \le x < 1 \quad \Longrightarrow \quad \begin{cases} W_{1,0}(x) = \sqrt{2}, \\ W_{1,1}(x) = 2\cos(2\pi(2x-1)), \\ W_{1,2}(x) = 2\sin(2\pi(2x-1)). \end{cases} \end{cases} \tag{2.8}$$

So, with the collocation points

$$x_m = \frac{2m-1}{2\mathcal{N}}, \qquad m = 1, 2, \ldots, \mathcal{N} = 2^{\kappa}(2\ell+1), \tag{2.9}$$

the graphs of $W_{r,s}(x)$ for $\kappa = \ell = 1$, are shown in Fig. 2.1.

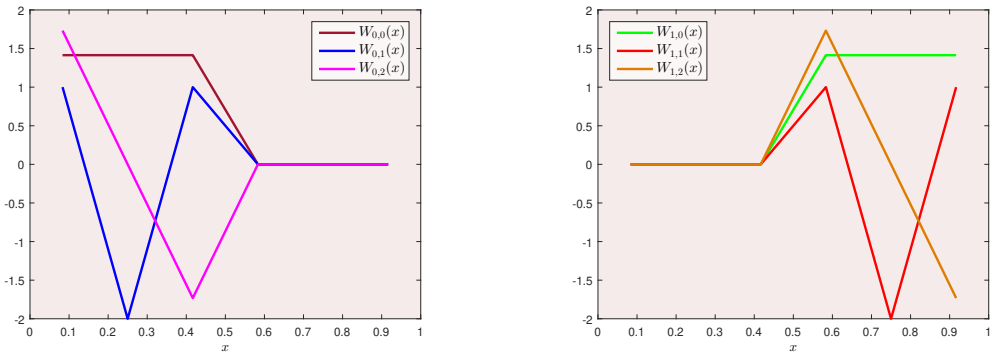

Fig. 2.1. The graphs of $W_{r,s}(x)$ for $\kappa = \ell = 1$.

2.1. Expanding functions into the SCWs

Using the set of SCWs, any function $\Upsilon(x) \in \mathcal{L}^2([0,1))$ can be approximated as an infinite series of these functions as follows:

$$\Upsilon(x) = \sum_{r=0}^{\infty} \sum_{s=0}^{2\ell} a_{r,s} W_{r,s}(x), \tag{2.10}$$

where $a_{r,s} =< \Upsilon, W_{r,s} >= \int_0^1 \Upsilon(x) W_{r,s}(x)\, dx$. By truncating the infinite series (2.10) at levels $r = 2^{\kappa} - 1$ and $s = 2\ell$, we obtain an approximate representation for $\Upsilon(x)$ as

$$\Upsilon(x) \simeq \sum_{r=0}^{2^{\kappa}-1} \sum_{s=0}^{2\ell} a_{r,s} W_{r,s}(x) = \mathcal{A}^T \Gamma(x), \tag{2.11}$$

where $\mathcal{A}$ and Γ are $(\mathcal{N} \times 1)$-vectors and are introduced as follows:

$$\begin{aligned} \mathcal{A} &= \left[a_{0,0}, a_{0,1}, \ldots, a_{0,2\ell}, a_{1,0}, a_{1,1}, \ldots, a_{1,2\ell}, \ldots\ldots, a_{2^{\kappa}-1,0}, a_{2^{\kappa}-1,1} \ldots, a_{2^{\kappa}-1,2\ell}\right]^T, \\ \Gamma &= \left[W_{0,0}, W_{0,1}, \ldots, W_{0,2\ell}, W_{1,0}, W_{1,1}, \ldots, W_{1,2\ell}, \ldots\ldots, W_{2^{\kappa}-1,0}(x), W_{2^{\kappa}-1,1} \ldots, W_{2^{\kappa}-1,2\ell}\right]^T. \end{aligned} \tag{2.12}$$

The SCWs matrix $\Gamma_{\mathcal{N}\times\mathcal{N}}$ at the collocation points (2.9), is given as follows:

$$\Gamma_{\mathcal{N}\times\mathcal{N}} = \left[\Gamma\Big(\frac{1}{2\mathcal{N}}\Big), \Gamma\Big(\frac{3}{2\mathcal{N}}\Big), \ldots, \Gamma\Big(\frac{2\mathcal{N}-1}{2\mathcal{N}}\Big)\right],$$

in other words

$$\Gamma_{\mathcal{N}\times\mathcal{N}} = \begin{bmatrix} W_{0,0}(\frac{1}{2\mathcal{N}}) & W_{0,0}(\frac{3}{2\mathcal{N}}) & \ldots & W_{0,0}(\frac{2\mathcal{N}-1}{2\mathcal{N}}) \\ W_{0,1}(\frac{1}{2\mathcal{N}}) & W_{0,1}(\frac{3}{2\mathcal{N}}) & \ldots & W_{0,1}(\frac{2\mathcal{N}-1}{2\mathcal{N}}) \\ \vdots & \vdots & \ldots & \vdots \\ W_{0,2\ell}(\frac{1}{2\mathcal{N}}) & W_{0,2\ell}(\frac{3}{2\mathcal{N}}) & \ldots & W_{0,2\ell}(\frac{2\mathcal{N}-1}{2\mathcal{N}}) \\ W_{1,0}(\frac{1}{2\mathcal{N}}) & W_{1,0}(\frac{3}{2\mathcal{N}}) & \ldots & W_{1,0}(\frac{2\mathcal{N}-1}{2\mathcal{N}}) \\ W_{1,1}(\frac{1}{2\mathcal{N}}) & W_{1,1}(\frac{3}{2\mathcal{N}}) & \ldots & W_{1,1}(\frac{2\mathcal{N}-1}{2\mathcal{N}}) \\ \vdots & \vdots & \ldots & \vdots \\ W_{1,2\ell}(\frac{1}{2\mathcal{N}}) & W_{1,2\ell}(\frac{3}{2\mathcal{N}}) & \ldots & W_{1,2\ell}(\frac{2\mathcal{N}-1}{2\mathcal{N}}) \\ \vdots & \vdots & \ldots & \vdots \\ \vdots & \vdots & \ldots & \vdots \\ W_{2^\kappa-1,0}(\frac{1}{2\mathcal{N}}) & W_{2^\kappa-1,0}(\frac{3}{2\mathcal{N}}) & \ldots & W_{2^\kappa-1,0}(\frac{2\mathcal{N}-1}{2\mathcal{N}}) \\ W_{2^\kappa-1,1}(\frac{1}{2\mathcal{N}}) & W_{2^\kappa-1,1}(\frac{3}{2\mathcal{N}}) & \ldots & W_{2^\kappa-1,1}(\frac{2\mathcal{N}-1}{2\mathcal{N}}) \\ \vdots & \vdots & \ldots & \vdots \\ W_{2^\kappa-1,2\ell}(\frac{1}{2\mathcal{N}}) & W_{2^\kappa-1,2\ell}(\frac{3}{2\mathcal{N}}) & \ldots & W_{2^\kappa-1,2\ell}(\frac{2\mathcal{N}-1}{2\mathcal{N}}) \end{bmatrix}.$$

In particular, for $\kappa = \ell = 1$, the SCWs matrix $\Gamma_{6\times6}$ is given as follows:

$$\Gamma_{6\times6} = \begin{bmatrix} \sqrt{2} & \sqrt{2} & \sqrt{2} & 0 & 0 & 0 \\ 1 & -2 & 1 & 0 & 0 & 0 \\ \sqrt{3} & 0 & -\sqrt{3} & 0 & 0 & 0 \\ 0 & 0 & 0 & \sqrt{2} & \sqrt{2} & \sqrt{2} \\ 0 & 0 & 0 & 1 & -2 & 1 \\ 0 & 0 & 0 & \sqrt{3} & 0 & -\sqrt{3} \end{bmatrix}.$$

2.2. The operational matrix of SCWs

Due to the vector form (2.12), the integration of $\Gamma(x)$ can be calculated as follows:

$$\int_0^x \Gamma(t)\,dt = \mathcal{Q}\Gamma(x),$$

where $\mathcal{Q}$ is $\mathcal{N}\times\mathcal{N}$ operational matrix given by

$$\mathcal{Q} = \frac{1}{2^{\kappa+\frac{1}{2}}} \begin{pmatrix} \mathcal{F} & \mathcal{S} & \cdots & \mathcal{S} \\ 0 & \mathcal{F} & \cdots & \mathcal{S} \\ \vdots & \vdots & \ddots & \vdots \\ 0 & 0 & \cdots & \mathcal{F} \end{pmatrix},$$

where $\mathcal{S}$ and $\mathcal{F}$ are $(2\ell+1)\times(2\ell+1)$ matrices (see [15]).

3. APPLICATION OF THE METHOD

In this section, we use the SCWs method for finding the approximate solutions of system (1.1) with specified initial and boundary conditions (1.2) and (1.3). For this, dividing the interval $[0, t_{fin}]$ into $\mathcal{M}$ equal parts of length $\hbar_t = \frac{t_{fin}}{\mathcal{M}}$ and denoting $t_n = (n-1)\hbar_t$, $n = 1, 2, \ldots, (\mathcal{M}+1)$, we expand $\dot{\Psi}'$ and $\dot{\Phi}'''$ in terms of SCWs as,

$$\dot{\Psi}'(x,t) \cong \sum_{r=0}^{2^\kappa - 1} \sum_{s=0}^{2\ell} a_{r,s} W_{r,s}(x) = \mathcal{A}^T \Gamma(x), \tag{3.13}$$

$$\dot{\Phi}'''(x,t) \cong \sum_{r=0}^{2^\kappa - 1} \sum_{s=0}^{2\ell} b_{r,s} W_{r,s}(x) = \mathcal{B}^T \Gamma(x), \tag{3.14}$$

where *prime* and *dot* mean differentiation concerning x and t, respectively. Now, we consider the following two cases:
Case 1: Considering the equation (3.13): By integrating this equation once concerning t from t_n to t and once concerning x from 0 to x, we have

$$\Psi'(x,t) = (t - t_n)\mathcal{A}^T \Gamma(x) + \Psi'(x, t_n), \tag{3.15}$$

$$\dot{\Psi}(x,t) = \mathcal{A}^T \mathcal{Q} \Gamma(x) + g_1'(t), \tag{3.16}$$

Now, integrating equation (3.16) once concerning t from t_n to t, we obtain

$$\Psi(x,t) = (t - t_n)\mathcal{A}^T \mathcal{Q} \Gamma(x) + [g_1(t) - g_1(t_n)] + \Psi(x, t_n). \tag{3.17}$$

Case 2: Considering the equation (3.14): By integrating this equation once concerning t from t_n to t and three times concerning x from 0 to x, we obtain

$$\Phi'''(x,t) = (t - t_n)\mathcal{B}^T \Gamma(x) + \Phi'''(x, t_n), \tag{3.18}$$

$$\Phi'(x,t) = (t - t_n)\mathcal{B}^T \mathcal{Q}^2 \Gamma(x) + \Phi'(x, t_n) + [w_2(t) - w_2(t_n)] + x[\dot{\Phi}''(0,t) - \dot{\Phi}''(0, t_n)], \tag{3.19}$$

$$\Phi(x,t) = (t - t_n)\mathcal{B}^T \mathcal{Q}^3 \Gamma(x) + \Phi(x, t_n) + [g_2(t) - g_2(t_n)] + x[w_2(t) - w_2(t_n)] + \frac{x^2}{2}[\dot{\Phi}''(0,t) - \dot{\Phi}''(0, t_n)], \tag{3.20}$$

$$\dot{\Phi}(x,t) = \mathcal{B}^T \mathcal{Q}^3 \Gamma(x) + g_2'(t) + x w_2'(t) + \frac{x^2}{2}\dot{\Phi}''(0,t). \tag{3.21}$$

By using the boundary condition $\Phi(1,t) = k_2(t)$ equations (3.19)-(3.21) are changed as follows:

$$\Phi'(x,t) = (t - t_n)\mathcal{B}^T \mathcal{Q}^2 \Gamma(x) + \Phi'(x, t_n) + (1 - 2x)[w_2(t) - w_2(t_n)] + 2x[k_2(t) - k_2(t_n)] - 2x[g_2(t) - g_2(t_n)], \tag{3.22}$$

$$\Phi(x,t) = (t - t_n)\mathcal{B}^T \mathcal{Q}^3 \Gamma(x) + \Phi(x, t_n) + (1 - x^2)[g_2(t) - g_2(t_n)] + x(1 - x)[w_2(t) - w_2(t_n)] + x^2[k_2(t) - k_2(t_n)], \tag{3.23}$$

$$\dot{\Phi}(x,t) = \mathcal{B}^T \mathcal{Q}^3 \Gamma(x) + (1 - x^2) g_2'(t) + x(1 - x) w_2'(t) + x^2 k_2'(t). \tag{3.24}$$

Discretizing the results (3.15)-(3.17) and (3.18) and (3.22)-(3.24), by assuming $x \to x_m$ and $t \to t_{n+1}$, we have

$$\Psi'(x_m,t_{n+1}) = \hbar_t \mathcal{A}^T \Gamma(x_m) + \Psi'(x_m,t_n), \tag{3.25}$$
$$\dot{\Psi}(x_m,t_{n+1}) = \mathcal{A}^T \mathcal{Q}\Gamma(x_m) + g_1'(t_{n+1}), \tag{3.26}$$
$$\Psi(x_m,t_{n+1}) = \hbar_t \mathcal{A}^T \mathcal{Q}\Gamma(x) + [g_1(t_{n+1}) - g_1(t_n)] + \Psi(x_m,t_n), \tag{3.27}$$
$$\Phi'''(x_m,t_{n+1}) = \hbar_t \mathcal{B}^T \Gamma(x_m) + \Phi'''(x_m,t_n), \tag{3.28}$$
$$\begin{aligned}\Phi'(x_m,t_{n+1}) &= \hbar_t \mathcal{B}^T \mathcal{Q}^2 \Gamma(x_m) + \Phi'(x_m,t_n) + (1-2x_m)[w_2(t_{n+1}) - w_2(t_n)] \\ &\quad + 2x_m[k_2(t_{n+1}) - k_2(t_n)] - 2x_m[g_2(t_{n+1}) - g_2(t_n)],\end{aligned} \tag{3.29}$$
$$\begin{aligned}\Phi(x_m,t_{n+1}) &= \hbar_t \mathcal{B}^T \mathcal{Q}^3 \Gamma(x_m) + \Phi(x_m,t_n) + (1-x_m^2)[g_2(t_{n+1}) - g_2(t_n)] \\ &\quad + x_m(1-x_m)[w_2(t_{n+1}) - w_2(t_n)] + x_m^2[k_2(t_{n+1}) - k_2(t_n)],\end{aligned} \tag{3.30}$$
$$\dot{\Phi}(x_m,t_{n+1}) = \mathcal{B}^T \mathcal{Q}^3 \Gamma(x_m) + (1-x_m^2) g_2'(t_{n+1}) + x_m(1-x_m) w_2'(t_{n+1}) + x_m^2 k_2'(t_{n+1}), \tag{3.31}$$

where, x_m's are the collocation points that are introduced in (2.9). To linearized the nonlinear terms $\Phi\Phi_x$, $\Psi_x\Phi$, and $\Psi\Phi_x$ in system (1.1), we use the linearization form given by Rubin and Graves [21] as follows:

$$\Phi\Phi_x = \Phi_x(x,t_n)\Phi(x,t_{n+1}) - \Phi_x(x,t_n)\Phi(x,t_n) + \Phi(x,t_n)\Phi_x(x,t_{n+1}), \tag{3.32}$$
$$\Psi_x\Phi = \Phi(x,t_n)\Psi_x(x,t_{n+1}) - \Phi(x,t_n)\Psi_x(x,t_n) + \Psi_x(x,t_n)\Phi(x,t_{n+1}), \tag{3.33}$$
$$\Psi\Phi_x = \Phi_x(x,t_n)\Psi(x,t_{n+1}) - \Phi_x(x,t_n)\Psi(x,t_n) + \Psi(x,t_n)\Phi_x(x,t_{n+1}). \tag{3.34}$$

Using linear expressions (3.32)-(3.34), the discrete form of system (1.1) considering x_m and t_{n+1} is as follows:

$$\begin{cases} \dot{\Psi}(x_m,t_{n+1}) + \alpha\Phi'(x_m,t_n)\Phi(x_m,t_{n+1}) + \alpha\Phi(x_m,t_n)\Phi'(x_m,t_{n+1}) = \alpha\Phi'(x_m,t_n)\Phi(x_m,t_n), \\ \\ \dot{\Phi}(x_m,t_{n+1}) + \beta\Phi'''(x_m,t_{n+1}) + \delta\Phi(x_m,t_n)\Psi'(x_m,t_{n+1}) + \delta\Psi'(x_m,t_n)\Phi(x_m,t_{n+1}) \\ +\gamma\Phi'(x_m,t_n)\Psi(x_m,t_{n+1}) + \gamma\Psi(x_m,t_n)\Phi'(x_m,t_{n+1}) = \delta\Phi(x_m,t_n)\Psi'(x_m,t_n) \\ +\gamma\Phi'(x_m,t_n)\Psi(x_m,t_n). \end{cases} \tag{3.35}$$

Now, by using equations (3.25)-(3.31), system (3.35) leads to

$$\begin{cases} \mathcal{A}^T\theta_1 + \mathcal{B}^T\theta_2 = \mathcal{H}_1(x_m,t_n), \\ \mathcal{A}^T\theta_3 + \mathcal{B}^T\theta_4 = \mathcal{H}_2(x_m,t_n), \end{cases} \tag{3.36}$$

where the matrices θ_i, $i = 1,2,3,4$ are matrices with dimensions $\mathcal{N} \times \mathcal{N}$ as follows:

$$\theta_1 = \mathcal{Q}\Gamma(x_m),$$
$$\theta_2 = \Big[\alpha\Phi'(x_m,t_n)\hbar_t\mathcal{Q}^3\Gamma(x_m) + \alpha\Phi(x_m,t_n)\hbar_t\mathcal{Q}^2\Gamma(x_m)\Big],$$
$$\theta_3 = \Big[\delta\Phi(x_m,t_n)\hbar_t\Gamma(x_m) + \gamma\Phi'(x_m,t_n)\hbar_t\mathcal{Q}\Gamma(x_m)\Big],$$
$$\theta_4 = \Big[\mathcal{Q}^3\Gamma(x_m) + \beta\hbar_t\Gamma(x_m) + \delta\Psi'(x_m,t_n)\hbar_t\mathcal{Q}^3\Gamma(x_m) + \gamma\Psi(x_m,t_n)\hbar_t\mathcal{Q}^2\Gamma(x_m)\Big],$$

and the matrices $\mathcal{H}_i$, $i = 1, 2$ are matrices with dimensions $\mathcal{N} \times 1$ as follows:

$$\begin{aligned}\mathcal{H}_1(x_m, t_n) =& -\alpha\Phi(x_m, t_n)\Phi'(x_m, t_n) - g_1'(t_{n+1}) - \alpha\Phi'(x_m, t_n)\Big[(1 - x_m^2)[g_2(t_{n+1}) - g_2(t_n)]\\ &+ x_m(1 - x_m)[w_2(t_{n+1}) - w_2(t_n)] + x_m^2[k_2(t_{n+1}) - k_2(t_n)]\Big]\\ &- \alpha\Phi(x_m, t_n)\Big[(1 - 2x_m)[w_2(t_{n+1}) - w_2(t_n)] + 2x_m[k_2(t_{n+1}) - k_2(t_n)]\\ &- 2x_m[g_2(t_{n+1}) - g_2(t_n)]\Big],\end{aligned}$$

$$\begin{aligned}\mathcal{H}_2(x_m, t_n) =& -\beta\Phi'''(x_m, t_n) - \delta\Phi(x_m, t_n)\Psi'(x_m, t_n)\\ &- \gamma\Phi'(x_m, t_n)[g_1(t_{n+1}) - g_1(t_n) + \Psi(x_m, t_n)]\\ &- \Big[(1 - x_m^2)g_2'(t_{n+1}) + x_m(1 - x_m)w_2'(t_{n+1}) + x_m^2k_2'(t_{n+1})\Big]\\ &- \delta\Psi'(x_m, t_n)\Big[(1 - x_m^2)[g_2(t_{n+1}) - g_2(t_n)] + x_m(1 - x_m)[w_2(t_{n+1}) - w_2(t_n)]\\ &+ x_m^2[k_2(t_{n+1}) - k_2(t_n)]\Big] - \gamma\Psi(x_m, t_n)\Big[(1 - 2x_m)[w_2(t_{n+1}) - w_2(t_n)]\\ &+ 2x_m[k_2(t_{n+1}) - k_2(t_n)] - 2x_m[g_2(t_{n+1}) - g_2(t_n)]\Big].\end{aligned}$$

The matrix-vector form of system (3.36) is as follows:

$$\left[\begin{array}{c:c}\theta_1 & \theta_2\\ \hdashline \theta_3 & \theta_4\end{array}\right]_{2\mathcal{N}\times 2\mathcal{N}} \left[\begin{array}{c}\mathcal{A}\\ \hdashline \mathcal{B}\end{array}\right]_{2\mathcal{N}\times 1} = \left[\begin{array}{c}\mathcal{H}_1\\ \hdashline \mathcal{H}_2\end{array}\right]_{2\mathcal{N}\times 1} \tag{3.37}$$

From (3.37), the coefficients vector $\mathcal{A}$ and $\mathcal{B}$ can be calculated. With these coefficients and using the equations (3.27) and (3.30), the approximate solutions are successively obtained.

4. NUMERICAL EXPERIMENTS

In this section, we apply the SCWs method to obtain the numerical solutions of the DSW system (1.1). To compare the obtained numerical results, we use the following solutions that obtained by Arnous et al. ([1]):

$$\begin{cases}\Psi(x, t) = \frac{6c}{\gamma+2\delta}\text{sech}^2\Big(\sqrt{\frac{c}{\beta k^2}}(k(x - ct) - \xi_0)\Big),\\ \\ \Phi(x, t) = \pm\sqrt{\frac{12c^2}{\alpha(\gamma+2\delta)}}\text{sech}\Big(\sqrt{\frac{c}{\beta k^2}}(k(x - ct) - \xi_0)\Big),\end{cases}$$

where c and k are arbitrary real constants.
To show the effectiveness and accuracy of the proposed method, we considered an example with $\alpha = \beta = \gamma = \delta = 1$, $t_{fin} = 1$, $\hbar_t = 0.01$.

Remark 4.1:
For describing the error, we introduce the infinity-norm of absolute error and the root mean square (RMS) error norm as follows:

$$\begin{aligned}L_\infty^\Psi &= ||\Psi(x_m, t) - \Psi^*(x_m, t)||_\infty = \max_{1\le m\le\mathcal{N}}|\Psi(x_m, t) - \Psi^*(x_m, t)|,\\ RMS^\Psi &= \left[\frac{1}{2\mathcal{N}}\sum_{m=1}^{2\mathcal{N}}\Big(\Psi(x_m, t) - \Psi^*(x_m, t)\Big)^2\right]^{\frac{1}{2}},\end{aligned} \tag{4.38}$$

where Ψ^* is the approximate solution of Ψ. Similarly, the L_∞^Φ and RMS$^\Phi$ are obtained according to formulas (4.38).

The numerical results for $\Psi(x,t)$ and $\Phi(x,t)$ at time $t=1$ when $\ell=\kappa=1$ are reported in Table 4.1. For different values of κ, Table 4.2 stated the calculated errors (4.38) at time $t=0.5$, also, the execution times for these values are given in Table 4.3. Difference between exact and numerical solutions Ψ and Φ at time $t=1$ are shown in Figs. 4.2-4.4 and 4.5-4.7, respectively.

Table 4.1. The numerical results for $\Psi(x,t)$ and $\Phi(x,t)$ at $t=1$ when $\ell=\kappa=1$.

x_m	$\Psi(x_m,1)$	$\Psi^*(x_m,1)$	$\lvert\Psi(x_m,1)-\Psi^*(x_m,1)\rvert$	$\Phi(x_m,1)$	$\Phi^*(x_m,1)$	$\lvert\Phi(x_m,1)-\Phi^*(x_m,1)\rvert$
0.0833333	0.153514	0.153517	$2.358647e-06$	0.159955	0.159953	$2.434473e-06$
0.25	0.157382	0.157384	$2.526247e-06$	0.161958	0.161949	$8.477983e-06$
0.416667	0.160643	0.160646	$2.873385e-06$	0.163627	0.163619	$7.684178e-06$
0.583333	0.163242	0.163244	$2.279712e-06$	0.164945	0.164933	$1.248603e-05$
0.75	0.165133	0.165128	$5.211826e-06$	0.165898	0.165906	$7.514665e-06$
0.916667	0.166281	0.166280	$1.685403e-06$	0.166474	0.166457	$1.740170e-05$

Table 4.2. The calculated errors (4.38) at time $t=0.5$ with $\ell=1$.

		$\Psi(x,0.5)$	$\Phi(x,0.5)$
L_∞	$\kappa=1$	$1.333830e-06$	$8.630715e-06$
	$\kappa=2$	$6.055654e-08$	$1.078673e-06$
	$\kappa=3$	$2.810132e-09$	$7.847945e-08$
	$\kappa=4$	$8.968863e-11$	$5.304455e-09$
	$\kappa=5$	$3.105035e-12$	$3.172111e-10$
	$\kappa=6$	$9.736049e-14$	$2.018670e-11$
RMS	$\kappa=1$	$7.661924e-07$	$5.199718e-06$
	$\kappa=2$	$3.315228e-08$	$5.115186e-07$
	$\kappa=3$	$1.000311e-09$	$2.933696e-08$
	$\kappa=4$	$3.271928e-11$	$2.026272e-09$
	$\kappa=5$	$9.981293e-13$	$1.217716e-10$
	$\kappa=6$	$3.154537e-14$	$7.797156e-12$

Table 4.3. The execution times for different values of κ with $\ell=1$.

	$\kappa=1$	$\kappa=2$	$\kappa=3$	$\kappa=4$	$\kappa=5$	$\kappa=6$
CPU time (s)	102.835546	189.641444	373.585049	753.232887	1519.095320	3163.873643

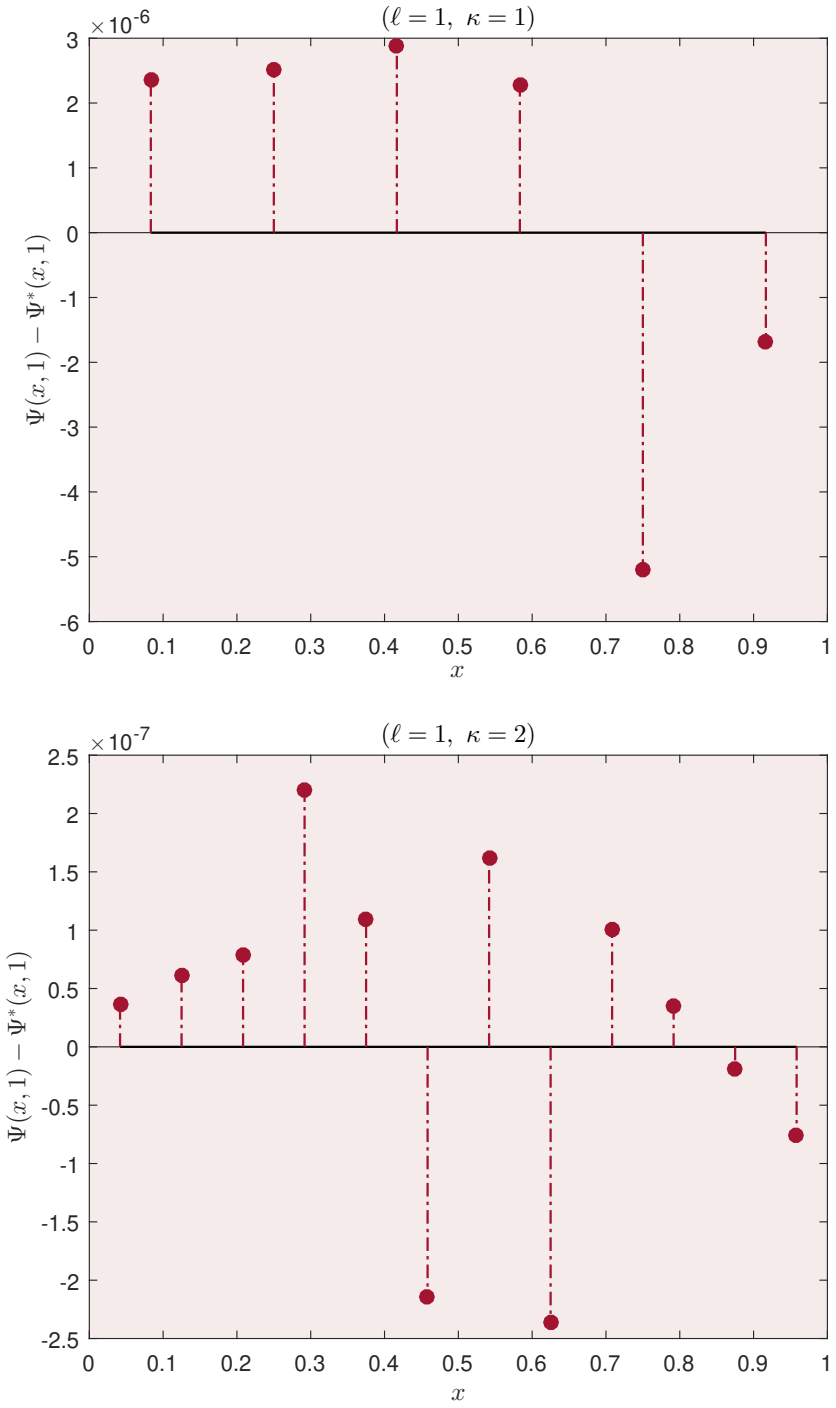

Fig. 4.2. Difference between exact and numerical solutions Ψ at time $t = 1$, when $\ell = 1$ and $\kappa = 1, 2$.

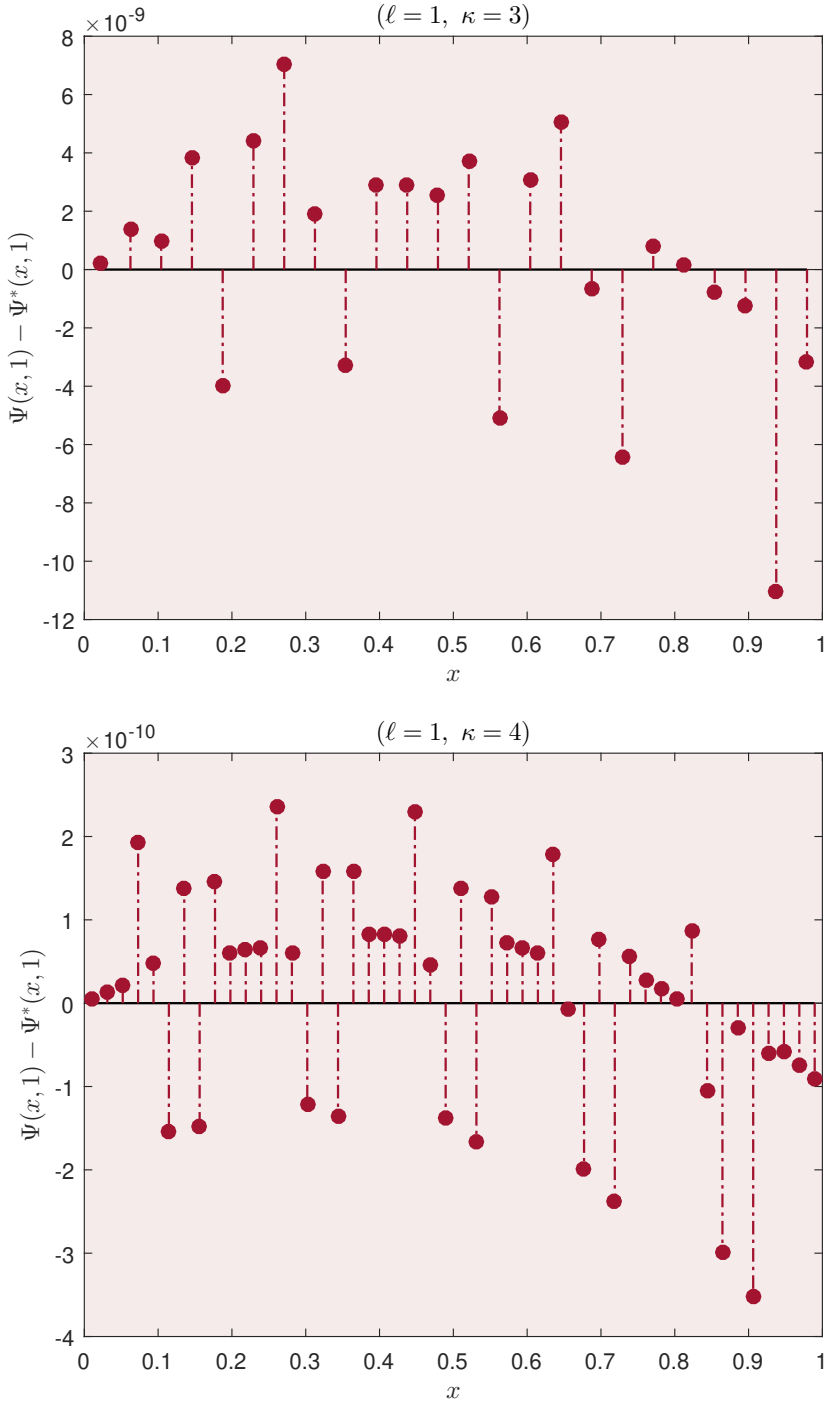

Fig. 4.3. Difference between exact and numerical solutions Ψ at time $t = 1$, when $\ell = 1$ and $\kappa = 3, 4$.

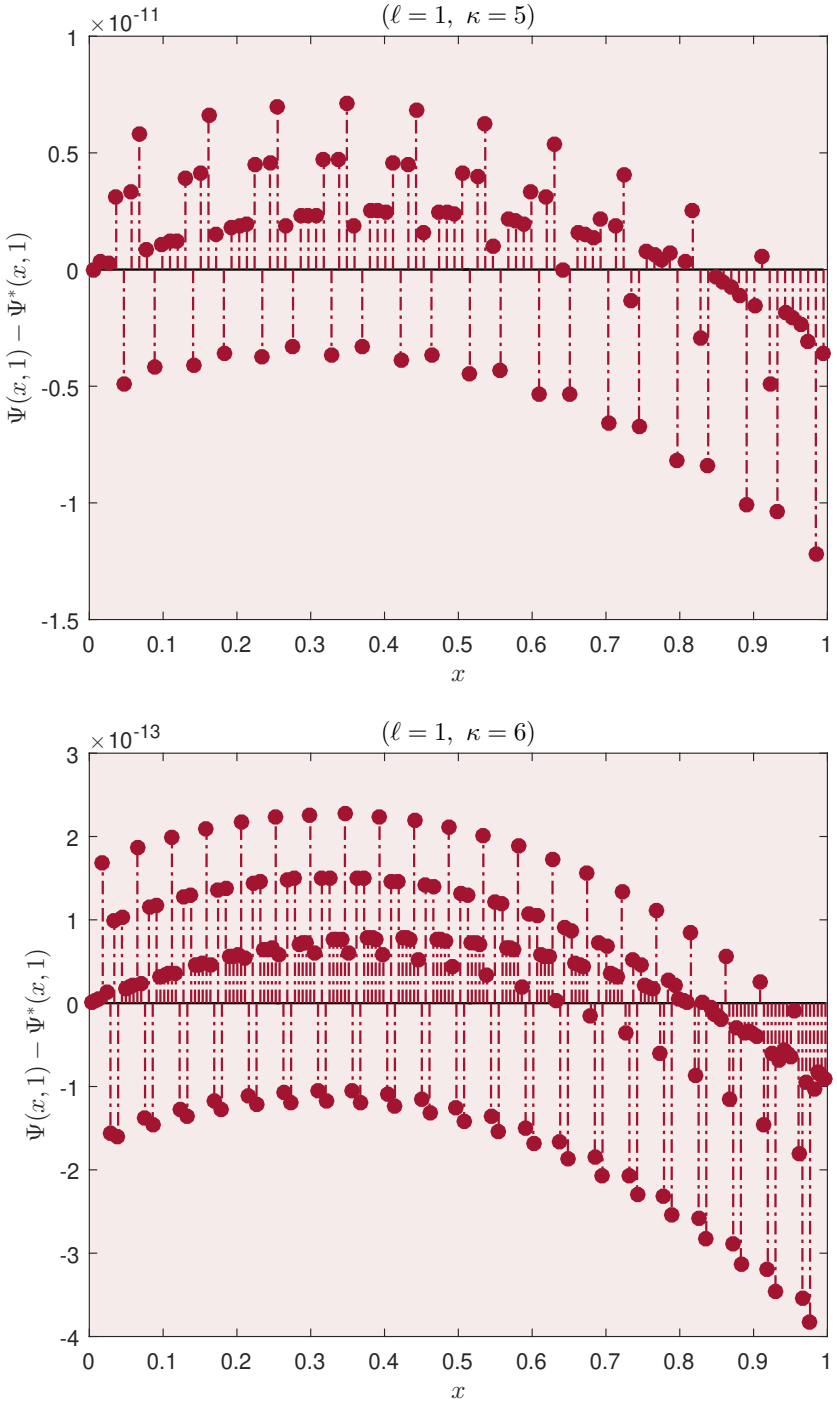

Fig. 4.4. Difference between exact and numerical solutions Ψ at time $t = 1$, when $\ell = 1$ and $\kappa = 5, 6$.

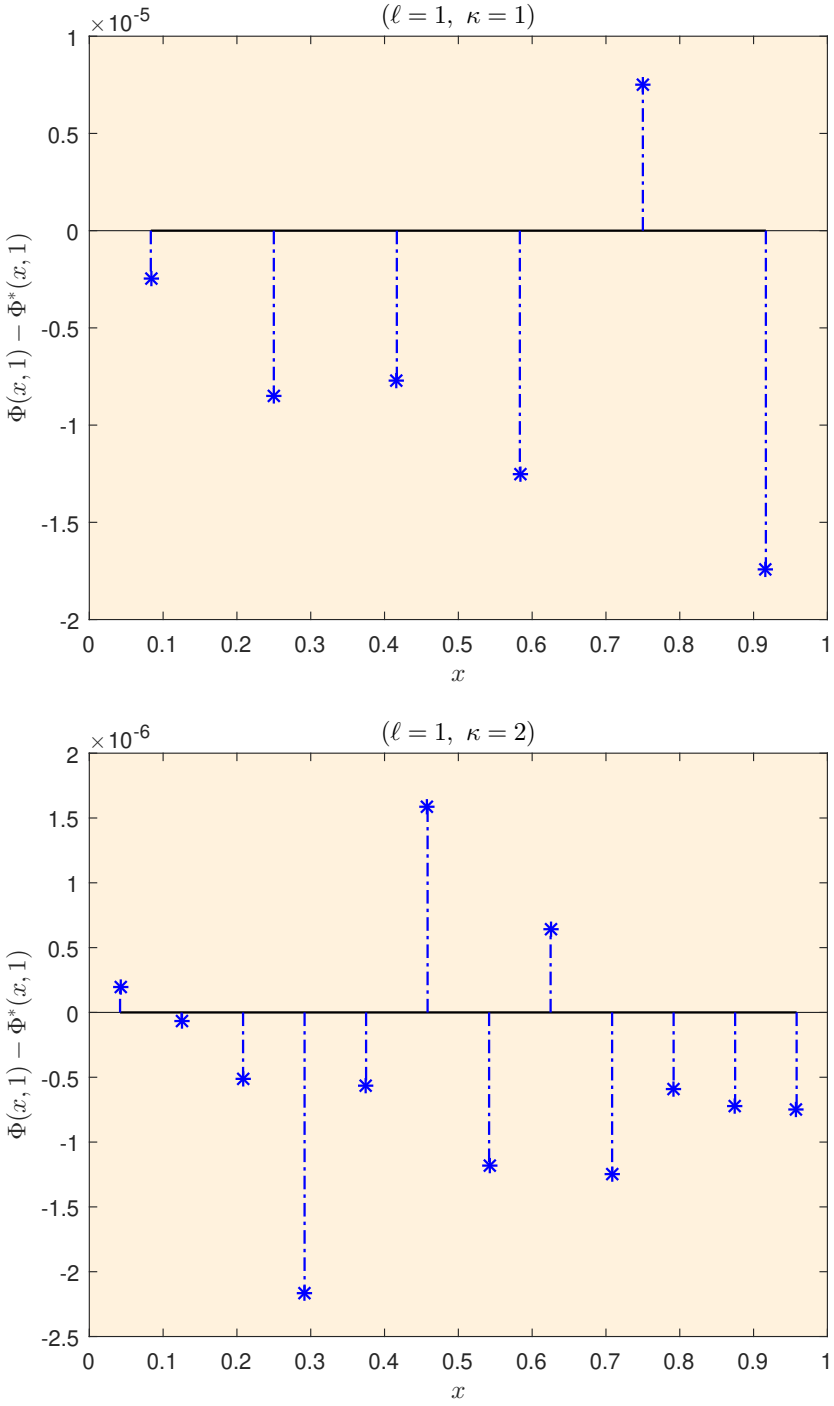

Fig. 4.5. Difference between exact and numerical solutions Φ at time $t = 1$, when $\ell = 1$ and $\kappa = 1, 2$.

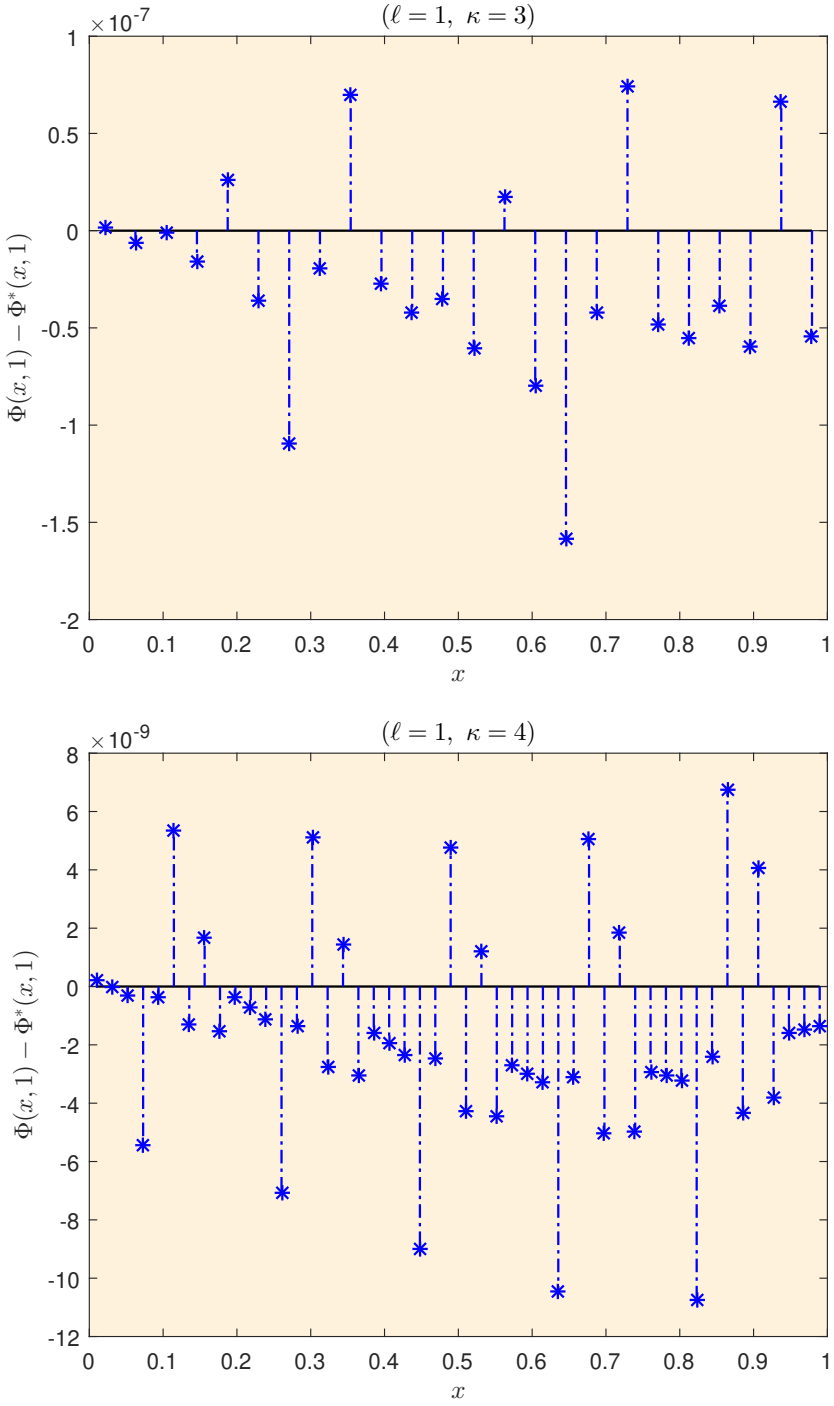

Fig. 4.6. Difference between exact and numerical solutions Φ at time $t = 1$, when $\ell = 1$ and $\kappa = 3, 4$.

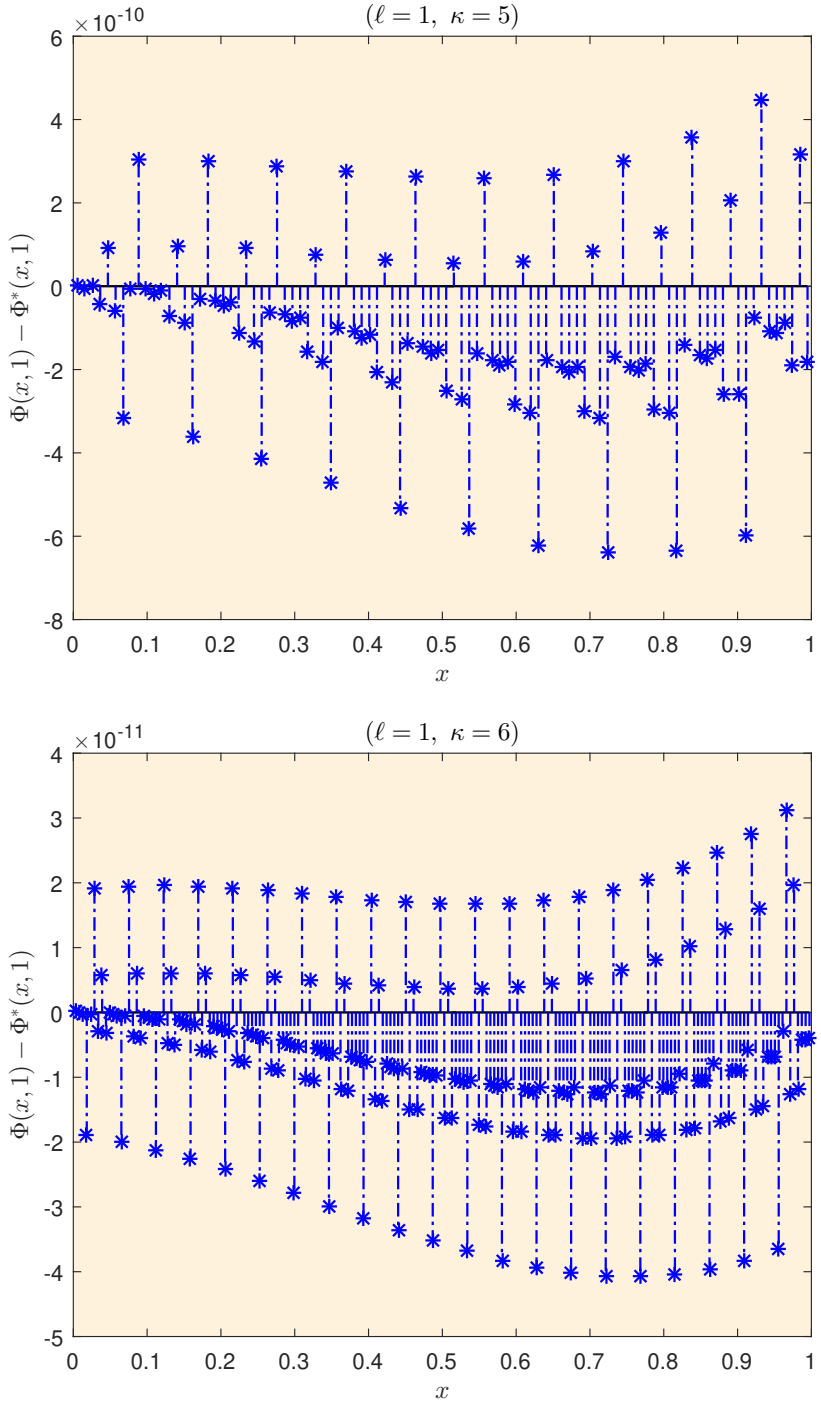

Fig. 4.7. Difference between exact and numerical solutions Φ at time $t = 1$, when $\ell = 1$ and $\kappa = 5, 6$.

Given the approximation function $\Upsilon(x)$ expressed in section 2, the solutions of the system (1.1), can be expanded as:

$$\Upsilon(x) = \sum_{r=0}^{\infty} \sum_{s=0}^{2\ell} a_{r,s} W_{r,s}(x). \tag{4.39}$$

In the investigated example, we approximate the solution of this equation as follows:

$$\Upsilon(x) \simeq \sum_{r=0}^{2^{\kappa}-1} \sum_{s=0}^{2\ell} a_{r,s} W_{r,s}(x), \tag{4.40}$$

which is the truncating the infinite series (4.39). By substituting the solutions $a_{r,s}$ in (4.40), we get the error function $\mathscr{E}(x)$ as follows:

$$\mathscr{E}(x) = \left| \Upsilon(x) - \sum_{r=0}^{2^{\kappa}-1} \sum_{s=0}^{2\ell} a_{r,s} W_{r,s}(x) \right|.$$

Therefore, as κ increases, the series (4.40) becomes larger and closer to the series (4.39), in other words, $\mathscr{E}(x)$ approaches zero. The obtained numerical results for Ψ and Φ confirm this.

5. CONCLUSION

In this article, using the SCWs method and using the initial and boundary conditions (1.2) and (1.3), we solved the DSW system (1.1) numerically. Considering the obtained numerical results in Tables 4.1 and 4.2, Figs. 4.2-4.7, and also comparing these results with the exact solutions, it can be concluded that the presented method for solving the DSW system (1.1) is an efficient and high accuracy method. The strength of this method is the simplicity of calculations with low storage space.

REFERENCES

1. Arnous, A., Mirzazadeh, M., & Eslami, M. (2016). Exact solutions of the Drinfel'd–Sokolov–Wilson equation using Bäcklund transformation of Riccati equation and trial function approach. *Pramana*, *86*(6), 1153–1160.
2. Aziz, I., Khan, F., et al. (2014). A new method based on Haar wavelet for the numerical solution of two-dimensional nonlinear integral equations. *Journal of Computational and Applied Mathematics*, *272*, 70–80.
3. Chen, C., & Hsiao, C. (1997). Haar wavelet method for solving lumped and distributed-parameter systems. *IEE Proceedings-Control Theory and Applications*, *144*(1), 87–94.
4. Chui, C. K. (2016). *An introduction to wavelets*. Elsevier.
5. Daubechies, I. (1992). *Ten lectures on wavelets*. SIAM.
6. Daubechies, I., & Lagarias, J. C. (1992). Two-scale difference equations ii. local regularity, infinite products of matrices and fractals. *SIAM Journal on Mathematical Analysis*, *23*(4), 1031–1079.
7. Drinfeld, V. G., & Sokolov, V. V. (1981). Equations of Korteweg–De Vries type, and simple Lie algebras. In *Doklady Akademii Nauk*, 258, 11–16.
8. Drinfel'd, V. G., & Sokolov, V. V. (1985). Lie algebras and equations of Korteweg-De Vries type. *Journal of Soviet mathematics*, *30*(2), 1975–2036.
9. Foadian, S., Pourgholi, R., Tabasi, S. H., & Damirchi, J. (2019). The inverse solution of the coupled nonlinear reaction–diffusion equations by the Haar wavelets. *International Journal of Computer Mathematics*, *96*(1), 105–125.
10. Fu, Z., Yuan, N., Chen, Z., Mao, J., & Liu, S. (2009). Multi-order exact solutions to the Drinfel'd–Sokolov–Wilson equations. *Physics Letters A*, *373*(41), 3710–3714.
11. Heil, C. (1993). Ten lectures on wavelets (ingrid daubechies). *SIAM Review*, *35*(4), 666–669.
12. Hirota, R., Grammaticos, B., & Ramani, A. (1986). Soliton structure of the Drinfel'd–Sokolov–Wilson equation. *Journal of mathematical physics*, *27*(6), 1499–1505.

13. Hosseininia, M., Heydari, M., & Avazzadeh, Z. (2020). Numerical study of the variable-order fractional version of the nonlinear fourth-order 2d diffusion-wave equation via 2d Chebyshev wavelets. *Engineering with Computers*, 1–10.
14. Irfan, N., & Siddiqi, A. (2016). Sine-Cosine wavelets approach in numerical evaluation of Hankel transform for seismology. *Applied Mathematical Modelling*, *40*(7-8), 4900–4907.
15. Kajani, M. T., Ghasemi, M., & Babolian, E. (2006). Numerical solution of linear integro-differential equation by using Sine–Cosine wavelets. *Applied Mathematics and Computation*, *180*(2), 569–574.
16. Mallat, S. G. (2009). A theory for multiresolution signal decomposition: the wavelet representation. In *Fundamental Papers in Wavelet Theory*, 494–513.
17. Misirli, E., & Gurefe, Y. (2010). Exact solutions of the Drinfel'd–Sokolov–Wilson equation using the Exp-function method. *Applied Mathematics and Computation*, *216*(9), 2623–2627.
18. Pourgholi, R., Esfahani, A., Foadian, S., & Parehkar, S. (2013). Resolution of an inverse problem by Haar basis and Legendre wavelet methods. *International Journal of Wavelets, Multiresolution and Information Processing*, *11*(05), 1350034.
19. Pourgholi, R., Tavallaie, N., & Foadian, S. (2012). Applications of Haar basis method for solving some ill-posed inverse problems. *Journal of Mathematical Chemistry*, *50*(8), 2317–2337.
20. Razzaghi, M., & Yousefi, S. (2002). Sine-Cosine wavelets operational matrix of integration and its applications in the calculus of variations. *International Journal of Systems Science*, *33*(10), 805–810.
21. Rubin, S. G., & Graves Jr, R. A. (1975). A cubic spline approximation for problems in fluid mechanics. *NASA STI/Recon Technical Report N*, *75*, 33345.
22. Saeed, A., & Saeed, U. (2019). Sine-Cosine wavelet method for fractional oscillator equations. *Mathematical Methods in the Applied Sciences*, *42*(18), 6960–6971.
23. Wen, Z., Liu, Z., & Song, M. (2009). New exact solutions for the classical Drinfel'd–Sokolov–Wilson equation. *Applied Mathematics and Computation*, *215*(6), 2349–2358.
24. Wilson, G. (1982). The affine Lie algebra c (1) 2 and an equation of Hirota and Satsuma. *Physics Letters A*, *89*(7), 332–334.
25. Xiao-Xing, N., & Qing-Ping, L. (2015). Darboux transformation for Drinfel'd–Sokolov–Wilson equation. *Communications in Theoretical Physics*, *64*(5), 491.
26. Yang, Y., Heydari, M., Avazzadeh, Z., & Atangana, A. (2020). Chebyshev wavelets operational matrices for solving nonlinear variable-order fractional integral equations. *Advances in Difference Equations*, *2020*(1), 1–24.
27. Yuttanan, B., & Razzaghi, M. (2019). Legendre wavelets approach for numerical solutions of distributed order fractional differential equations. *Applied Mathematical Modelling*, *70*, 350–364.

